

A generic diffusion-based approach for 3D human pose prediction in the wild

Saeed Saadatnejad¹, Ali Rasekh, Mohammadreza Mofayez², Yasamin Medghalchi², Sara Rajabzadeh², Taylor Mordan¹ and Alexandre Alahi¹

Abstract—3D human pose forecasting, i.e., predicting a sequence of future human 3D poses given a sequence of past observed ones, is a challenging spatio-temporal task. It can be more challenging in real-world applications where occlusions will inevitably happen, and estimated 3D coordinates of joints would contain some noise. We provide a unified formulation in which incomplete elements (no matter in the prediction or observation) are treated as noise and propose a conditional diffusion model that denoises them and forecasts plausible poses. Instead of naively predicting all future frames at once, our model consists of two cascaded sub-models, each specialized for modeling short and long horizon distributions. We also propose a generic framework to improve any 3D pose forecasting model by leveraging our diffusion model in two additional steps: a pre-processing step to repair the inputs and a post-processing step to refine the outputs. We investigate our findings on four standard datasets (Human3.6M, HumanEva-I, AMASS, and 3DPW) and obtain significant improvements over the state-of-the-art. The code will be made available online upon publication.

I. INTRODUCTION

Nowadays, robots and humans work in proximity. To have safe and advanced interactions, the robots should understand the distribution of feasible human motions and accurately predict them. Thus, only predicting the location of a single point for each human is not enough. Instead, a more detailed representation, i.e., 3D human pose, should be targeted for the next generation of human-robot interactions.

Predicting 3D pose, the task of predicting a sequence of future 3D poses of a person given a sequence of past observed ones, is a challenging task to solve, as it mixes spatial and temporal reasoning and has multiple modes. While previous models have shown acceptable accurate predictions [32], [30], they perform poorly in imperfect observation settings. In the real world, noise exists in the perceived motion of a person due to sensor errors and occlusions by the same person, other objects in the scene, and other people.

Denoising Diffusion Probabilistic Models (DDPM) [21] are one kind of generative models that denoise input signal iteratively and have shown high-quality image synthesis [14]. Motivated by this property, we propose a diffusion model that explicitly handles noisy data input so it not only predicts accurate and in-distribution poses but can also be used in the wild. As depicted in Figure 1, we make a full sequence of observation and future frames by putting noise for the incomplete observation joints and future poses. This sequence is fed to our model for denoising, and in several steps, the correct

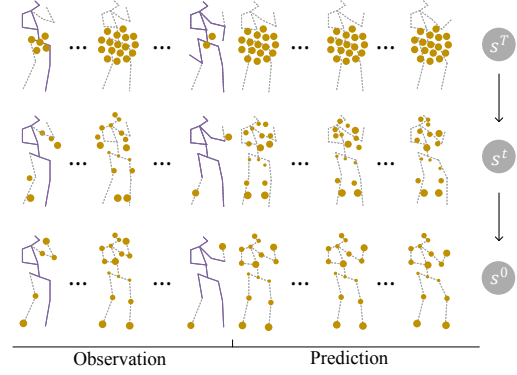


Fig. 1: Our conditional diffusion model denoises the input sequence s^T in T steps by 1) predicting poses for the future frames, and 2) repairing the imperfect observation when there is occlusion (the first column), missing whole frame (the second column), or noisy observation (third column). The big yellow circles represent the gaussian noise we consider for the unavailable joints, which gradually become small and fit to correct locations.

predictions and refinements are achieved. Naively predicting all future frames at once leads to inaccurate predictions in later frames, so we break the problem into two simpler tasks, and our model consists of two temporally cascaded diffusion blocks. The former predicts the short-term poses and repairs the imperfect observations (if applicable), and the latter takes the output of the former as a condition and predicts the long-term poses. We also extend our model to a generic framework that could improve the performance of the state-of-the-art models in a black-box manner. Leveraging our proposed model, we pre-process the imperfect observation and feed the pseudo-clean data to any prediction model to predict reasonably. Their predictions can be further enhanced using our model in post-processing.

To summarize, our contributions are three-fold. First, we propose a two-level diffusion model for long-term 3D human pose prediction in perfect and imperfect input observation settings. Second, we present a generic framework of pre-processing and post-processing leveraging our model that can be used with any pose prediction model. Finally, we perform extensive experiments and demonstrate our findings on several standard datasets (Human3.6M [22], HumanEva-I [43], AMASS [31] and 3DPW [46]), and obtain a significant improvement over the state-of-the-art. The code will be made available online upon publication.

¹EPFL, Lausanne, Switzerland

²Sharif University of Technology, Tehran, Iran

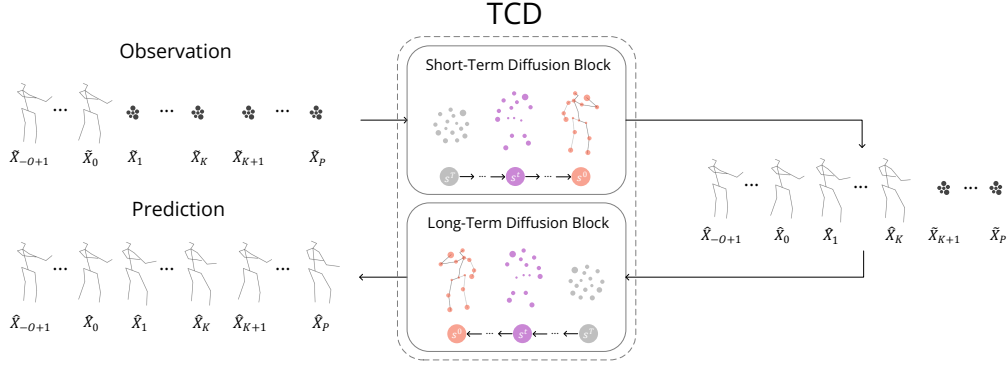


Fig. 2: Overview of our Temporal Cascaded Diffusion (TCD). The short-term diffusion block (top) takes the observed sequence padded with random noise and predicts short-term human poses in K frames. The predicted sequence along with the observation padded with random noise are given to the long-term diffusion block (bottom) to predict for all P frames.

II. RELATED WORK

The task of 3D pose forecasting is a long-standing problem. Recurrent Neural Networks (RNNs) have been widely used [16], [23], [35], [9], [17], [10] as they are capable of capturing the temporal dependencies in sequential data, and some used only feed-forward networks [25]. Later, Graph Convolutional Networks (GCN) could better capture the spatial dependencies of body poses [34], [13], [32], [27]. Separating temporal and spatial convolution blocks [30], and trainable adjacency matrices [44], [51] are among other proposed ideas. Attention-based approaches have recently gained interest for modeling human motion [36], [39] and HRI [32] showed a huge improvement by spatio-temporal self-attention module. We leverage attention in our proposed model. While some have used context information [8], [19], [11], social interactions [1] or action class [2], [7], in this paper, we focus on conditioning on just observation sequence.

Deterministic models provide relatively accurate predictions; however, they lack diverse and multi-modal predictions compared to stochastic models [50], [4], [3], [42], [29], [33]. In this category, Variational AutoEncoders (VAEs) have been widely used considering their strengths in learning representations [38], [50], [4], [3]. With the emergence of denoising diffusion probabilistic models (DDPM) [21] as a generative model capable of modeling the data distribution and their success in image synthesis [14], image repainting [28] and text to image [41], [40], recently people used it for time-series imputation [45], i.e., repairing the missing elements. However, they have not studied the human motion prediction problem. To the best of our knowledge, we are the first to propose a stochastic diffusion model for human pose prediction which outperforms both stochastic and diffusion prediction models.

Previous models perform poorly in incomplete observation. Recently, a multi-task learning approach was proposed that can work in imperfect observation settings and implicitly ignores noise in data [12]. However, we explicitly denoise the input leading to a generalizable solution. We could also better capture the spatio-temporal relationship, and the results will

be compared. Moreover, we provide a generic framework that can improve any state-of-the-art model in a black-box manner.

III. METHOD

A. Problem Definition and Notations

Let $X = [X_{-O+1}, X_{-O+2}, \dots, X_0, X_1, \dots, X_P] \in \mathbb{R}^{(O+P) \times J \times 3}$ be a clean complete normalized sequence of human body poses with J joints in O frames of observation and P frames of future. Each joint consists of its 3D cartesian coordinates. The availability mask is a binary matrix $M \in \{0, 1\}^{(O+P) \times J \times 3}$ where zero determines the parts of the sequence that are not observed due to occlusions or being from future timesteps. Note that the elements of M correspondent to P future frames are always zero. With this notation, the observed sequence $\hat{X} = [\hat{X}_{-O+1}, \hat{X}_{-O+2}, \dots, \hat{X}_0, \hat{X}_1, \dots, \hat{X}_P]$ is derived by applying the element-wise product of M into X and adding a Gaussian noise $\epsilon \sim \mathcal{N}(0, I)$ in non-masked area $\hat{X} = M \odot X + (1 - M)\epsilon$. The model predicts $\hat{X} = [\hat{X}_{-O+1}, \hat{X}_{-O+2}, \dots, \hat{X}_0, \hat{X}_1, \dots, \hat{X}_P]$ and the objective is lowering $|\hat{X} - X| \odot (1 - M)$ given \hat{X} .

B. Conditional Diffusion Blocks

We propose a conditional diffusion block inspired by [45]. It has multiple residual layers and each layer contains two cascaded transformers with the same input and output shapes. The temporal transformer is responsible for modeling the temporal behavior of data. Its output is fed to the spatial transformer for attending to the body pose inside each frame.

At training time, a gaussian noise with zero mean and pre-defined variance is added to the input pose sequence s^0 to make it noisier s^1 . This process is repeated for T steps following the Markov chain, thus, the output s^T will be close to a pure gaussian noise in the non-masked area:

$$q(s^t | s^{t-1}) = M \odot s^0 + (1 - M) \odot \mathcal{N}(s^t; \sqrt{1 - \beta^t} s^{t-1}, \beta^t \mathbf{I}), \quad (1)$$

where β^t the variance of the noise in step t is determined using a scheduler. We utilize the cosine noise scheduler, first

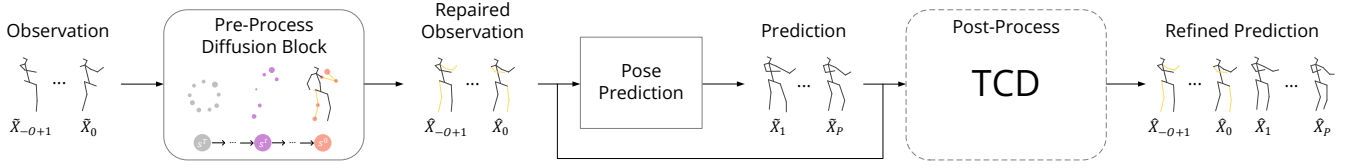


Fig. 3: An illustration of the pre-processing and post-processing framework. The pre-process diffusion block denoises the imperfect observation sequence. The repaired observation is then given to a frozen predictor. The output of the predictor model is passed to TCD to perform the post-processing step and refine its predictions.

introduced in [37]:

$$\beta^t = 1 - \frac{f(t)}{f(t-1)}, \quad f(t) = \cos^2\left(\frac{t/T + 0.008}{1 + 0.008} \cdot \frac{\pi}{2}\right). \quad (2)$$

Using the above function helps in slowly decreasing the quality of the input compared to commonly used schedulers like quadratic and linear. Therefore, the input information remains longer and the variances of noises are learned more accurately. The network learns to reverse the diffusion process and retrieve the clean sequence by predicting the cumulative noise that is added to s^t as described in DDPM [21].

At inference time, the model starts from an incomplete noisy observed sequence s^T , where we put a gaussian noise in the non-masked area and observation in the masked area. Then, it predicts the poses $s^{T-1} \dots s^0$ through an iterative process in which we subtract the learned additive noise at each step from the output of the previous iteration until it yields a clean output close to the ground truth.

C. Temporal Cascaded Diffusion (TCD)

We illustrate our main model, which consists of a short-term and a long-term diffusion blocks in Figure 2. The first block is specialized for pose prediction in the short term. The input of this block is \tilde{X} and the model predicts the first K frames of the future $\hat{X}_1 \dots \hat{X}_K$ and completes the observation frames $[\hat{X}_{-O+1} \dots \hat{X}_0]$. The task of the second block is to predict the rest of the future frames $[\hat{X}_{K+1} \dots \hat{X}_P]$ given the observation and the output of the first block. Note that two sub-models are trained separately using clean complete input, but in inference time, the average of 5 samples of the short-term block is given to the long-term predictor.

Cascading two diffusion models results in better overall and specifically long-term prediction because of dividing the challenging behavior. In other words, the short-term prediction block focuses on predicting a few samples, and thanks to its accurate short-term predictions, the long-term prediction block receives more information to attend to and puts its capacity in longer horizons.

D. Pre-processing and Post-processing

Given a frozen pose prediction model, we can improve its performance by repairing the input sequence in pre-processing and finetuning its outputs in post-processing. This framework is shown in Figure 3.

a) *Pre-Processing*: Since most of the existing pose prediction models cannot handle imperfect observations, we propose a simpler version of our model as a pre-processing step to denoise the observation only. This module takes the imperfect observed sequence $[\tilde{X}_{-O+1}, \tilde{X}_{-O+2}, \dots, \tilde{X}_0]$ as input and repairs it to $[\hat{X}_{-O+1}, \hat{X}_{-O+2}, \dots, \hat{X}_0]$. The architecture is similar to TCD yet predicts in one level, and the input and output sequences have O frames. Our accurate repairing enables any pose prediction model trained on complete data to predict reasonably.

b) *Post-Processing*: Furthermore, we want to improve the prediction results of existing models. We feed the results of any black-box pose prediction model $[\tilde{X}_1, \dots, \tilde{X}_P]$ concatenated with repaired observation $[\hat{X}_{-O+1}, \hat{X}_{-O+2}, \dots, \hat{X}_0]$ as the input to our TCD and retrain it to predict better. The initial prediction acts as the starting point where our post-processing gradually shifts it towards the real distribution.

IV. EXPERIMENTS

A. Experimental Setup

1) *Datasets*: We compare all approaches on four standard 3D human pose forecasting datasets.

Human3.6M [22] is the largest benchmark dataset for human motion analysis, with 3.6 million body poses. It comprises 15 complex action categories, each one performed by seven actors individually. The validation set is subject-11, the test set is subject-5, and all the remaining five subjects are training samples. The original 3D pose skeletons in the dataset consist of 32 joints. Previous works reported their performances in different settings. To have a thorough and correct comparison, we define the following settings:

- **Setting-A**: 25 observation frames, 100 prediction frames at 50 fps (frame per second), with the subset of 17 joints to represent the human pose;
- **Setting-B**: 50 observation frames, 25 prediction frames down-sampled to 25 fps, with the subset of 22 joints to represent the human pose;
- **Setting-C**: 25 observation frames, 25 prediction frames down-sampled to 25 fps, with the subset of 17 joints.

We train our models on all action classes at the same time.

AMASS (The Archive of Motion Capture as Surface Shapes) [31] is a recently published human motion dataset that unifies 18 motion capture datasets totaling 13,944 motion sequences from 460 subjects performing a large variety

Model	Human3.6M [22]					HumanEva-I [43]		
	APD \uparrow	ADE \downarrow	FDE \downarrow	MMADE \downarrow	MMFDE \downarrow	APD \uparrow	ADE \downarrow	FDE \downarrow
Pose-Knows [47]	6723	461	560	522	569	2308	269	296
MT-VAE [48]	403	457	595	716	883	21	345	403
HP-GAN [5]	7214	858	867	847	858	1139	772	749
BoM [6]	6265	448	533	514	544	2846	271	279
GMVAE [15]	6769	461	555	524	566	2443	305	345
DeLiGAN [18]	6509	483	534	520	545	2177	306	322
DSF [49]	9330	493	592	550	599	4538	273	290
DLow [50]	11741	425	518	495	531	4855	251	268
Motron [42]	7168	375	488	—	—	—	—	—
Multi-Objective [29]	14240	414	516	—	—	5786	228	236
GSPS [33]	14757	389	496	476	525	5825	233	244
TCD (ours)	19466	356	396	463	445	6764	199	215

TABLE I: Comparison with stochastic models on Human3.6M [22] Setting-A and HumanEva-I [43] at a horizon of 2s.

of actions. We use 50 observation frames down-sampled to 25fps with 18 joints, similar to previous works.

3DPW (3D Poses in the Wild) [46] is the first dataset with accurate 3D poses in the wild. It contains 60 video sequences taken from a moving phone camera. Each pose is described as an 18-joint skeleton with 3D coordinates similar to AMASS dataset. We use the official instructions to obtain training, validation, and test sets.

HumanEva-I [43] includes 3 subjects that perform different actions captured at 60fps. Each person has 15 body joints. We remove the global translation and use the official train/test split of the dataset. In this dataset, the prediction horizon is 60 frames (1s) given 15 observed frames (0.25s) similar to [33].

2) *Other Implementation Details:* Our network is optimized with Adam [24], with a batch size of 32 and a learning rate of 0.001, decayed by a factor of 0.1 at 75% and 90% of the total epochs. Our diffusion model has 12 layers of residual blocks and 50 steps. In TCD, the length of short-term prediction K is 20% of the total prediction length P . Each transformer has 64 channels and 8 attention heads.

3) *Evaluation Metrics:* We measure the Displacement Error (DE), in millimeters (mm), over all joints in a frame and report the Average Displacement Error (ADE) as the average of DE for the whole sequence and the Final Displacement Error (FDE) as DE in the final predicted frame. Similar to [33], we also report the multi-modal versions of ADE (MMADE) and FDE (MMFDE). We follow the same evaluation protocol as in [50] to measure diversity and report the Average Pairwise Distance (APD) between different predictions.

B. Baselines

We compare our results with several recent methods, including stochastic approaches [33], [50], [42], [29] and deterministic approaches [35], [25], [34], [32], [30], [44], [51] when possible as the settings are not the same and some of them are not open-source. We also consider *Zero-Vel* as a competitive baseline. *Zero-Vel* is a simple model that outputs the last observed pose as the predictions for all future poses.

C. Comparisons with the State of the Art

We separate our experiments into three different settings: we first compare to other stochastic approaches, then to deterministic ones, and finally evaluate on imperfect scenarios with incomplete or noisy observation data.

1) *Comparisons with Stochastic Approaches:* We evaluate our model on two datasets, Human3.6M [22] Setting-A and HumanEva-I [43], and compare it with other stochastic approaches in Table I. Each model is sampled 50 times given each observation sequence. TCD (ours) clearly performs better than previous works in terms of the accuracy of the best sample (ADE and FDE) and multiple samples (MMADE and MMFDE) while generating diverse poses (APD).

2) *Comparisons with Deterministic Approaches:* We then compare our model to deterministic approaches on Human3.6M [22] Setting-B in Table II. To compare with deterministic models, ours is sampled 5 times, and the best sample is considered. Our model performs better than previous works in the short-term and with a larger margin in the long-term, thanks to our two-level prediction. The detailed results on all categories of Human3.6M in addition to comparisons with models that did not report in standard settings, are available in the appendix.

We also report the results of two previous state-of-the-art models post-processed by our generic framework at the bottom of Table II. Note that as input data is complete, we only add post-processing (TCD) to their outputs. The improvements from our generic framework are non-negligible and could even beat our original model. It is more evident for longer horizons caused by our two-level prediction. This table shows that starting with a better initial guess, the pose sequence can be better shifted towards the real distribution.

The large long-term improvement can be observed in AMASS [31] and 3DPW [46], too. Similar to previous works, we train our model on AMASS and measure FDE on both datasets. The comparison with models that reported in this setting is shown in Table III.

Qualitative results on Human3.6M are shown in Figure 4. Predictions from our model are displayed along with predictions from several baselines and are superimposed on the ground-truth poses for direct comparison. Our model has

Model	80ms	320ms	560ms	720ms	880ms	1000ms
Zero-Vel	23.8	76.0	107.4	121.6	131.6	136.6
Res. Sup. [35]	25.0	77.0	106.3	119.4	130.0	136.6
ConvSeq2Seq [25]	16.6	61.4	90.7	104.7	116.7	124.2
LTD-50-25 [34]	12.2	50.7	79.6	93.6	105.2	112.4
HRI [32]	10.4	47.1	77.3	91.8	104.1	112.1
PGBIG [30]	10.3	46.6	76.3	90.9	102.6	110.0
TCD (ours)	9.9	48.8	73.7	84.0	94.3	103.3
HRI [32] + TCD (ours)	10.3	47.3	72.9	83.8	94.0	102.9
PGBIG [30] + TCD (ours)	10.2	46.1	72.4	83.6	93.9	102.8

TABLE II: Comparison with deterministic models on Human3.6M [22] Setting-B in FDE (mm) at different horizons.

Model	AMASS [31]				3DPW [46]			
	560ms	720ms	880ms	1000ms	560ms	720ms	880ms	1000ms
Zero-Vel	130.1	135.0	127.2	119.4	93.8	100.4	102.0	101.2
convSeq2Seq [25]	79.0	87.0	91.5	93.5	69.4	77.0	83.6	87.8
LTD-10-25 [34]	57.2	65.7	71.3	75.2	57.9	65.8	71.5	75.5
HRI [32]	51.7	58.6	63.4	67.2	56.0	63.6	69.7	73.7
TCD (ours)	49.8	54.5	60.1	66.7	55.4	61.6	67.9	73.4

TABLE III: Comparison with deterministic models on AMASS [31] and 3DPW [46] in FDE (mm) at long horizons.

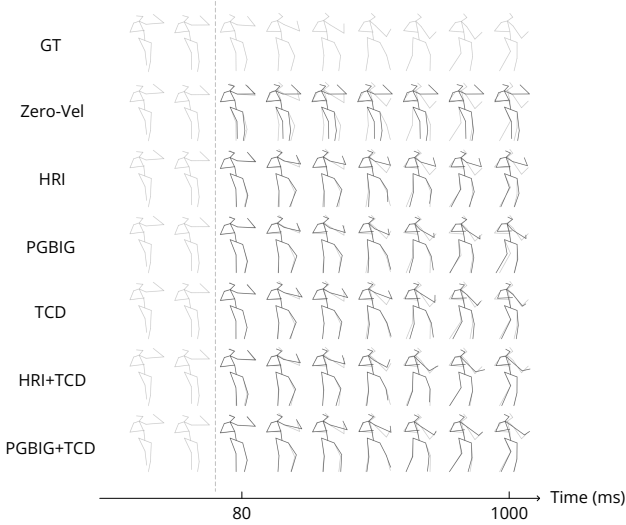


Fig. 4: Qualitative results on Human3.6M [22] Setting-B. For each row, the left part is the input observation, and the predicted poses superimposed on the ground truth are displayed on the right.

correctly learned the data distribution and predicts accurate and plausible poses. For instance, hand movement is natural when the feet move, while HRI shows fixed hands and PGBIG has a momentum that avoids large hand movements. In addition, the post-processing could shift the predicted pose more toward the ground truth.

3) *Comparisons on Imperfect Observation Data:* We now look at how models perform with imperfect observation data. This is a more realistic scenario than assuming perfect inputs, as occlusions would happen, and the estimated 3D coordinates of joints would contain some noise in practice. We start by randomly removing 40% of the left arm and right leg from the observations of Human3.6M Setting-B, at both

Model	80ms	320ms	560ms	720ms	880ms	1000ms
Zero-Vel	84.9	138.2	169.9	184.2	193.7	198.2
HRI [32]	65.2	104.5	130.0	141.6	151.1	157.1
PGBIG [30]	67.0	107.1	132.1	143.5	152.9	158.8
TCD (ours)	11.2	51.3	75.4	85.4	95.4	104.5
Pre(ours) + Zero-Vel	24.1	76.3	107.6	121.7	131.7	136.7
Pre(ours) + HRI [32]	11.4	48.6	78.3	92.7	105.0	112.8
Pre(ours) + PGBIG [30]	11.1	47.9	77.2	91.7	103.5	110.8
Pre(ours) + TCD (ours)	10.8	49.9	74.4	84.9	95.1	104.2

TABLE IV: Comparison on imperfect observation data and pre-processed observation data (Pre(ours)+) on Human3.6M [22] Setting-B in FDE (mm) at different horizons.

training and evaluation, to simulate occlusions. The state-of-the-art performs poorly on imperfect observation, as shown in the top half of Table IV, while ours perform close to the perfect input observation. If our pre-processing module is added to generate pseudo-perfect observation feeding to the state-of-the-art models and Zero-Vel, the performances significantly improve. MT-GCN [12] predicts in incomplete observation settings and reported the performance of some previous models when the input is repaired using their own method and the results on Human3.6M Setting-C is in the first column of Table V. Ours outperforms MT-GCN by a significant margin of 33.2mm in FDE at 1s horizon (30% improvement).

We analyze the performance of our model in several occlusion patterns masks M applied to input data:

- Random Leg, Arm Occlusions: leg and arm joints are randomly occluded with the same probability of 40%;
- Structured Joint Occlusions: 40% of the right leg joints for consecutive frames are missing;
- Missing Frames: 20% of consecutive frames are missing;
- Noisy Inputs: Gaussian noise with a standard deviation of $\sigma = 25$ or $\sigma = 50$ is added to the coordinates of the

Model	Random Leg, Arm Occlusions	Structured Joint Occlusions	Missing Frames	Noisy Inputs $\sigma = 25$ $\sigma = 50$	
R+TrajGCN [34]	121.1	131.5	–	127.1	135.0
R+LDRGCN [13]	118.7	127.1	–	126.4	133.6
R+DMGCN [26]	117.6	126.5	–	124.4	132.7
R+STMIGAN [20]	129.5	128.2	–	–	–
MT-GCN [12]	110.7	114.5	122.0	114.3	119.7
TCD (ours)	77.5	77.2	80.5	81.9	84.9

TABLE V: Comparison on imperfect observation data on Human3.6M [22] Setting-C in FDE (mm) at a horizon of 1s. Models in the top part of the table receive repaired sequences (R+), while others receive imperfect sequences.

Model	Train and Test Missing Ratio			
	10%	20%	30%	40%
MT-GCN [12]	109.4 / 8.6	110.5 / 13.7	112.3 / 18.7	114.4 / 24.5
TCD (ours)	77.1 / 2.2	77.2 / 2.3	77.6 / 2.6	79.1 / 2.9

TABLE VI: Results of motion prediction and sequence repairing on Human3.6M [22] Setting-C with varying amounts of randomly occluded joints in input data in FDE (mm) at a horizon of 1s / ADE (mm) of missing elements.

joints, and 50% of the leg joints are randomly occluded.

Table V presents the results when training and evaluating in the above observation patterns, in FDE at a prediction horizon of 1 second on Human3.6M Setting-C. Our model outperforms previous works in different patterns of occlusions and noises in input that may happen in the real world. We observed that missing 5 consecutive frames is more problematic than missing a part of the body in 10 consecutive frames, as the network can recover the former with spatial information.

To have a thorough comparison with MT-GCN, we train 4 models on several percentages of random joints missing in the observation pose sequence, and the performances of sequence repairing (ADE of the occluded observation sequence) and motion prediction (FDE at the 1-second horizon) are presented in Table VI. Our model provides a negligible error of 2.9mm in repairing with 40% of all joints missing, while MT-GCN gives 24.5mm of error. In forecasting, ours achieves more than 31% lower FDE compared to MT-GCN.

Moreover, in inference time, our model performs well even if it has not observed that occlusion pattern in training time.

		Test Missing Ratio			
		0%	20%	50%	90%
Train Missing Ratio	20%	76.8 / –	77.2 / 2.3	79.9 / 5.2	159.3 / 114.7
	50%	78.7 / –	77.8 / 2.1	78.7 / 3.6	105.2 / 51.9
	90%	82.3 / –	82.3 / 3.1	82.9 / 4.3	89.5 / 21.8

TABLE VII: Results of motion prediction and sequence repairing on Human3.6M [22] Setting-C with varying proportions of randomly occluded joints between training and testing in FDE (mm) at a horizon of 1s / ADE (mm) of missing elements.

We show this in Table VII, where we train our model with varying percentage of random occluded joints and evaluate it with different percentages of random occlusion. We observe that less noise at test time than training naturally shows higher prediction and repairing performances, and more noise at test time than training weakens. On the other hand, learning on highly occluded observation data leads to a better generalization when testing with a similarly high level of occlusion but to a slight decrease in FDE when testing with low levels of occlusion. Our model is able to predict with 90% of missing input without a considerable degradation in performance. This can be a great benefit in real-world applications with imperfect data.

D. Ablations Studies

Here, we investigate different network design choices and report ADE (mm) on Human3.6M [22] Setting-B. The full model gives an ADE of 63.3mm. Predicting in one level, i.e., 100% at once without having short and long prediction blocks, can increase ADE to 65.5mm, mainly caused by wrong predictions in longer horizons. Predicting in 3 levels, i.e., predicting 20%, 20%, and 60% in a sequential manner, lowers the performance to 66.9 because cascading multiple stochastic processes generates either random results or not diverse. The same effect exists for K where a smaller $K = 2$ fades the benefit of 2-level prediction (ADE of 65.1mm) and a larger $K = 10$ makes the task of short-term prediction harder; thus, ADE increases to 66.6mm.

We have tested a quadratic scheduler instead of our cosine scheduler, and it increased ADE by 1mm. In our full model, we have used 12 residual layers in our diffusion blocks. Decreasing it to 4 residual layers lowers the performance by 3mm. We did not use more than 12 residual layers because of the large negative effect on sampling time. Moreover, we have done several experiments on the architecture of the transformers and observed that both spatial transformer and time transformer help in learning the spatio-temporal features of pose sequence, and eliminating them one at a time degrades ADE to 74.5mm and 261.1mm, respectively.

V. CONCLUSION

In this work, we have addressed the task of 3D human pose prediction in imperfect settings. For this, we have first proposed a stochastic diffusion model suitable to imperfect input data observations happening in the wild. Our model predicts future poses in two levels (short-term and long-term) to better capture human motion dynamics and yields state-of-the-art results on four datasets, including both clean and imperfect input settings. We have then leveraged it to create a generic framework easily applicable to any existing predictor in a black-box manner. It adds two additional stages: a pre-processing to rectify noisy observations before feeding them to the predictor, and a post-processing to finetune the predicted poses. This framework has been applied to several state-of-the-art models, including the one we propose, to demonstrate its generic effectiveness at enhancing any predictions on Human3.6M.

ACKNOWLEDGMENT

The authors would like to thank Mohammadhossein Bahari and Bastien Van Delft for their helpful comments. This project has received funding from the European Union's Horizon 2020 research and innovation programme under the Marie Skłodowska-Curie grant agreement No 754354.

REFERENCES

- [1] Vida Adeli, Ehsan Adeli, Ian Reid, Juan Carlos Niebles, and Hamid Reza Tofighi. Socially and contextually aware human motion and pose forecasting. *IEEE Robotics and Automation Letters*, 5(4):6033–6040, 2020.
- [2] Emre Aksan, Manuel Kaufmann, Peng Cao, and Otmar Hilliges. A spatio-temporal transformer for 3d human motion prediction. *International Conference on 3D Vision (3DV)*, 2021.
- [3] Sadegh Aliakbarian, Fatemeh Saleh, Lars Petersson, Stephen Gould, and Mathieu Salzmann. Contextually plausible and diverse 3d human motion prediction. In *Proceedings of the IEEE/CVF International Conference on Computer Vision (ICCV)*, pages 11333–11342, October 2021.
- [4] Sadegh Aliakbarian, Fatemeh Sadat Saleh, Mathieu Salzmann, Lars Petersson, and Stephen Gould. A stochastic conditioning scheme for diverse human motion prediction. In *Proceedings of the IEEE conference on Computer Vision and Pattern Recognition (CVPR)*, pages 5223–5232, 2020.
- [5] Emad Barsoum, John R. Kender, and Zicheng Liu. Hp-gan: Probabilistic 3d human motion prediction via gan. *2018 IEEE/CVF Conference on Computer Vision and Pattern Recognition Workshops (CVPRW)*, pages 1499–149909, 2018.
- [6] Apratim Bhattacharyya, Bernt Schiele, and Mario Fritz. Accurate and diverse sampling of sequences based on a “best of many” sample objective. *2018 IEEE/CVF Conference on Computer Vision and Pattern Recognition*, pages 8485–8493, 2018.
- [7] Yujun Cai, Yiwei Wang, Yiheng Zhu, Tat-Jen Cham, Jianfei Cai, Junsong Yuan, Jun Liu, Chuanxia Zheng, Sijie Yan, Henghui Ding, Xiaohui Shen, Ding Liu, and Nadia Magnenat Thalmann. A unified 3d human motion synthesis model via conditional variational autoencoder. In *Proceedings of the IEEE/CVF International Conference on Computer Vision (ICCV)*, pages 11645–11655, October 2021.
- [8] Zhe Cao, Hang Gao, Kartikeya Mangalam, Qi-Zhi Cai, Minh Vo, and Jitendra Malik. Long-term human motion prediction with scene context. In *European Conference on Computer Vision*, pages 387–404. Springer, 2020.
- [9] Yu-Wei Chao, Jimei Yang, Brian Price, Scott Cohen, and Jia Deng. Forecasting human dynamics from static images. In *Proceedings of the IEEE conference on Computer Vision and Pattern Recognition (CVPR)*, pages 548–556, 2017.
- [10] Hsu-kuang Chiu, Ehsan Adeli, Borui Wang, De-An Huang, and Juan Carlos Niebles. Action-agnostic human pose forecasting. In *2019 IEEE Winter Conference on Applications of Computer Vision (WACV)*, pages 1423–1432. IEEE, 2019.
- [11] Enric Corona, Albert Pumarola, Guillem Alenya, and Francesc Moreno-Noguer. Context-aware human motion prediction. In *Proceedings of the IEEE conference on Computer Vision and Pattern Recognition (CVPR)*, pages 6992–7001, 2020.
- [12] Qiongjie Cui and Huaijiang Sun. Towards accurate 3d human motion prediction from incomplete observations. In *Proceedings of the IEEE conference on Computer Vision and Pattern Recognition (CVPR)*, pages 4801–4810, June 2021.
- [13] Qiongjie Cui, Huaijiang Sun, and Fei Yang. Learning dynamic relationships for 3d human motion prediction. In *The IEEE/CVF Conference on Computer Vision and Pattern Recognition (CVPR)*, pages 6519–6527, 2020.
- [14] Prafulla Dhariwal and Alexander Nichol. Diffusion models beat gans on image synthesis. *Advances in Neural Information Processing Systems*, 34:8780–8794, 2021.
- [15] Nat Dilokthanakul, Pedro A. M. Mediano, Marta Garnelo, Matthew C. H. Lee, Hugh Salimbeni, Kai Arulkumaran, and Murray Shanahan. Deep unsupervised clustering with gaussian mixture variational autoencoders. *CoRR*, abs/1611.02648, 2016.
- [16] Katerina Fragkiadaki, Sergey Levine, Panna Felsen, and Jitendra Malik. Recurrent network models for human dynamics. In *Proceedings of the IEEE International Conference on Computer Vision (ICCV)*, pages 4346–4354, 2015.
- [17] Partha Ghosh, Jie Song, Emre Aksan, and Otmar Hilliges. Learning human motion models for long-term predictions. In *International Conference on 3D Vision (3DV)*, pages 458–466. IEEE, 2017.
- [18] Swaminathan Gurumurthy, Ravi Kiran Sarvadevabhatla, and R. Venkatesh Babu. Deligan: Generative adversarial networks for diverse and limited data. *2017 IEEE Conference on Computer Vision and Pattern Recognition (CVPR)*, pages 4941–4949, 2017.
- [19] Mohamed Hassan, Duygu Ceylan, Ruben Villegas, Jun Saito, Jimei Yang, Yi Zhou, and Michael J. Black. Stochastic scene-aware motion prediction. In *Proceedings of the IEEE/CVF International Conference on Computer Vision (ICCV)*, pages 11374–11384, October 2021.
- [20] Alejandro Hernandez, Jurgen Gall, and Francesc Moreno-Noguer. Human motion prediction via spatio-temporal inpainting. In *Proceedings of the IEEE/CVF International Conference on Computer Vision*, pages 7134–7143, 2019.
- [21] Jonathan Ho, Ajay Jain, and Pieter Abbeel. Denoising diffusion probabilistic models. *arXiv preprint arxiv:2006.11239*, 2020.
- [22] Catalin Ionescu, Dragos Papava, Vlad Olaru, and Cristian Sminchisescu. Human3.6m: Large scale datasets and predictive methods for 3d human sensing in natural environments. *IEEE Transactions on Pattern Analysis and Machine Intelligence*, 36(7):1325–1339, jul 2014.
- [23] Ashesh Jain, Amir R Zamir, Silvio Savarese, and Ashutosh Saxena. Structural-rnn: Deep learning on spatio-temporal graphs. In *Proceedings of the IEEE conference on Computer Vision and Pattern Recognition (CVPR)*, pages 5308–5317, 2016.
- [24] Diederik P. Kingma and Jimmy Ba. Adam: A method for stochastic optimization. In *Proceedings of the International Conference on Learning Representations (ICLR)*, 2015.
- [25] Chen Li, Zhen Zhang, Wee Sun Lee, and Gim Hee Lee. Convolutional sequence to sequence model for human dynamics. In *Proceedings of the IEEE Conference on Computer Vision and Pattern Recognition (CVPR)*, pages 5226–5234, 2018.
- [26] Maosen Li, Siheng Chen, Yangheng Zhao, Ya Zhang, Yanfeng Wang, and Qi Tian. Dynamic multiscale graph neural networks for 3d skeleton based human motion prediction. In *Proceedings of the IEEE/CVF Conference on Computer Vision and Pattern Recognition*, pages 214–223, 2020.
- [27] Zhengguang Liu, Pengxiang Su, Shuang Wu, Xuanjing Shen, Haipeng Chen, Yanbin Hao, and Meng Wang. Motion prediction using trajectory cues. In *Proceedings of the IEEE/CVF International Conference on Computer Vision (ICCV)*, pages 13299–13308, October 2021.
- [28] Andreas Lugmayr, Martin Danelljan, Andres Romero, Fisher Yu, Radu Timofte, and Luc Van Gool. Repaint: Inpainting using denoising diffusion probabilistic models. In *Proceedings of the IEEE/CVF Conference on Computer Vision and Pattern Recognition (CVPR)*, pages 11461–11471, June 2022.
- [29] Hengbo Ma, Jiachen Li, Ramtin Hosseini, Masayoshi Tomizuka, and Chihoi Choi. Multi-objective diverse human motion prediction with knowledge distillation. In *Proceedings of the IEEE/CVF Conference on Computer Vision and Pattern Recognition (CVPR)*, pages 8161–8171, June 2022.
- [30] Tiezheng Ma, Yongwei Nie, Chengjiang Long, Qing Zhang, and Guiqing Li. Progressively generating better initial guesses towards next stages for high-quality human motion prediction. In *Proceedings of the IEEE/CVF Conference on Computer Vision and Pattern Recognition (CVPR)*, pages 6437–6446, June 2022.
- [31] Naureen Mahmood, Nima Ghorbani, Nikolaus F. Troje, Gerard Pons-Moll, and Michael J. Black. Amass: Archive of motion capture as surface shapes. In *Proceedings of the IEEE/CVF International Conference on Computer Vision (ICCV)*, October 2019.
- [32] Wei Mao, Miaomiao Liu, and Mathieu Salzmann. History repeats itself: Human motion prediction via motion attention. In *European Conference on Computer Vision*, pages 474–489. Springer, 2020.
- [33] Wei Mao, Miaomiao Liu, and Mathieu Salzmann. Generating smooth pose sequences for diverse human motion prediction. In *Proceedings of the IEEE/CVF International Conference on Computer Vision*, pages 13309–13318, 2021.
- [34] Wei Mao, Miaomiao Liu, Mathieu Salzmann, and Hongdong Li. Learning trajectory dependencies for human motion prediction. In *Proceedings of the IEEE/CVF International Conference on Computer Vision (ICCV)*, October 2019.
- [35] Julieta Martinez, Michael J Black, and Javier Romero. On human motion prediction using recurrent neural networks. In *Proceedings of the IEEE conference on Computer Vision and Pattern Recognition (CVPR)*, pages 2891–2900, 2017.
- [36] Angel Martínez-González, Michael Villamizar, and Jean-Marc Odobez. Pose transformers (potr): Human motion prediction with

- non-autoregressive transformers. In *Proceedings of the IEEE/CVF International Conference on Computer Vision (ICCV) Workshops*, pages 2276–2284, October 2021.
- [37] Alexander Quinn Nichol and Prafulla Dhariwal. Improved denoising diffusion probabilistic models. In *International Conference on Machine Learning (ICML)*, pages 8162–8171. PMLR, 2021.
- [38] Behnam Parsaeifard, Saeed Saadatnejad, Yuejiang Liu, Taylor Mordan, and Alexandre Alahi. Learning decoupled representations for human pose forecasting. In *ICCVW*, pages 2294–2303, 2021.
- [39] Mathis Petrovich, Michael J. Black, and Gül Varol. Action-conditioned 3d human motion synthesis with transformer vae. In *Proceedings of the IEEE/CVF International Conference on Computer Vision (ICCV)*, pages 10985–10995, October 2021.
- [40] Robin Rombach, Andreas Blattmann, Dominik Lorenz, Patrick Esser, and Björn Ommer. High-resolution image synthesis with latent diffusion models. In *Proceedings of the IEEE/CVF Conference on Computer Vision and Pattern Recognition*, pages 10684–10695, 2022.
- [41] Chitwan Saharia, William Chan, Saurabh Saxena, Lala Li, Jay Whang, Emily Denton, Seyed Kamyar Seyed Ghasemipour, Burcu Karagol Ayan, S Sara Mahdavi, Rapha Gontijo Lopes, et al. Photorealistic text-to-image diffusion models with deep language understanding. *arXiv preprint arXiv:2205.11487*, 2022.
- [42] Tim Salzman, Marco Pavone, and Markus Ryhl. Motron: Multimodal probabilistic human motion forecasting. In *Proceedings of the IEEE/CVF Conference on Computer Vision and Pattern Recognition (CVPR)*, pages 6457–6466, June 2022.
- [43] L. Sigal, A. Balan, and M. J. Black. HumanEva: Synchronized video and motion capture dataset and baseline algorithm for evaluation of articulated human motion. *International Journal of Computer Vision*, 87(1):4–27, Mar. 2010.
- [44] Theodoros Sofianos, Alessio Sampieri, Luca Franco, and Fabio Galasso. Space-time-separable graph convolutional network for pose forecasting. In *Proceedings of the IEEE/CVF International Conference on Computer Vision (ICCV)*, pages 11209–11218, October 2021.
- [45] Yusuke Tashiro, Jianming Song, Yang Song, and Stefano Ermon. Csd: Conditional score-based diffusion models for probabilistic time series imputation. *Advances in Neural Information Processing Systems*, 34:24804–24816, 2021.
- [46] Timo von Marcard, Roberto Henschel, Michael J Black, Bodo Rosenhahn, and Gerard Pons-Moll. Recovering accurate 3d human pose in the wild using imus and a moving camera. In *Proceedings of the European Conference on Computer Vision (ECCV)*, pages 601–617, 2018.
- [47] Jacob Walker, Kenneth Marino, Abhinav Gupta, and Martial Hebert. The pose knows: Video forecasting by generating pose futures. In *Proceedings of the IEEE international conference on computer vision (ICCV)*, pages 3332–3341, 2017.
- [48] Xinchun Yan, Akash Rastogi, Ruben Villegas, Kalyan Sunkavalli, Eli Shechtman, Sunil Hadap, Ersin Yumer, and Honglak Lee. Mt-vae: Learning motion transformations to generate multimodal human dynamics. In *Proceedings of the European Conference on Computer Vision (ECCV)*, pages 265–281, 2018.
- [49] Ye Yuan and Kris Kitani. Diverse trajectory forecasting with deterministic point processes. *arXiv preprint arXiv:1907.04967*, 2019.
- [50] Ye Yuan and Kris Kitani. Dlow: Diversifying latent flows for diverse human motion prediction. In *Proceedings of the European Conference on Computer Vision (ECCV)*, 2020.
- [51] Chongyang Zhong, Lei Hu, Zihao Zhang, Yongjing Ye, and Shihong Xia. Spatio-temporal gating-adjacency gcnn for human motion prediction. In *Proceedings of the IEEE/CVF Conference on Computer Vision and Pattern Recognition (CVPR)*, pages 6447–6456, June 2022.

APPENDIX

Here, we extend our comparisons in [Section IV-C.2](#):

- 1) We have compared ours with the models that reported ADE in [Table VIII](#). Note that we changed our setting accordingly to predict 25 frames given 10 observation frames on Human3.6M dataset down-sampled to 25 fps with the subset of 22 joints (Setting-D). We followed the settings of [51], in which the models are evaluated on all actions except walking together. Ours outperforms those GCN-based models.

Model	80ms	160ms	320ms	400ms	560ms	1000ms
Zero-Vel	18.1	28.7	46.9	54.6	67.7	93.3
STSGCN [44]	10.2	17.3	33.5	38.9	51.7	77.3
GAGCN [51]	10.1	16.9	32.5	38.5	50.0	72.9
TCD (ours)	7.4	14.0	27.7	33.9	44.7	66.5

TABLE VIII: Comparison with deterministic models on Human3.6M [22] Setting-D in ADE (mm) at different prediction horizons.

Model	80ms	160ms	320ms	400ms	560ms	1000ms
Zero-Vel	17.1	31.9	54.8	63.8	78.3	100.0
LDRGCN [13]	10.7	22.5	45.1	55.8	–	97.8
MPT [27]	8.3	18.8	39.0	47.9	65.3	96.4
TCD (ours)	8.3	18.8	37.8	44.9	55.9	76.9

TABLE IX: Comparison with deterministic models on Human3.6M [22] Setting-E in FDE (mm) at different prediction horizons.

- 2) Another experiment was conducted to compare with others that reported their performances on Human3.6M Setting-E in [Table IX](#). Note that in this setting, 25 frames are predicted given 10 observation frames down-sampled to 25 fps with the subset of 17 joints. Again, ours outperforms them, especially in longer horizons.
- 3) In [Table II](#), we compared the performance of different models on Human3.6M [22] Setting-B. The detailed results on all categories are reported in [Table X](#). We observe that in almost all categories ours beat previous models.

scenarios	Walking						Eating						Smoking						Discussion					
millisecond	80	320	560	720	880	1000	80	320	560	720	880	1000	80	320	560	720	880	1000	80	320	560	720	880	1000
Res. Sup.	23.2	61.0	71.6	72.5	76.0	79.1	16.8	53.5	74.9	85.9	93.8	98.0	18.9	57.5	78.1	88.6	96.6	102.1	25.7	80.0	109.5	122.0	128.6	131.8
convSeq2Seq	17.7	56.3	72.2	77.2	80.9	82.3	11.0	40.7	61.3	72.8	81.8	87.1	11.6	41.3	60.0	69.4	77.2	81.7	17.1	64.8	98.1	112.9	123.0	129.3
LTD	12.3	39.4	50.7	54.4	57.4	60.3	7.8	31.3	51.5	62.6	71.3	75.8	8.2	32.8	50.5	59.3	67.1	72.1	11.9	55.1	88.9	103.9	113.6	118.5
HRI	10.0	34.2	47.4	52.1	55.5	58.1	6.4	28.7	50.0	61.4	70.6	75.7	7.0	29.9	47.6	56.6	64.4	69.5	10.2	52.1	86.6	102.2	113.2	119.8
PGBIG	10.6	36.6	49.1	53.0	56.0	58.6	6.3	28.7	49.2	60.4	68.9	73.9	7.1	30.1	49.2	58.9	66.4	71.2	9.9	50.9	86.2	102.3	112.8	118.4
Ours	9.9	35.7	44.1	46.2	49.8	53.6	6.1	29.0	44.5	52.0	59.2	65.1	6.6	31.4	47.6	55.2	62.4	68.1	9.6	54.9	85.7	96.2	103.6	110.9
scenarios	Directions						Greeting						Phoning						Posing					
millisecond	80	320	560	720	880	1000	80	320	560	720	880	1000	80	320	560	720	880	1000	80	320	560	720	880	1000
Res. Sup.	21.6	72.1	101.1	114.5	124.5	129.5	31.2	96.3	126.1	138.8	150.3	153.9	21.1	66.0	94.0	107.7	119.1	126.4	29.3	98.3	140.3	159.8	173.2	183.2
convSeq2Seq	13.5	57.6	86.6	99.8	109.9	115.8	22.0	82.0	116.9	130.7	142.7	147.3	13.5	49.9	77.1	92.1	105.5	114.0	16.9	75.7	122.5	148.8	171.8	187.4
LTD	8.8	46.5	74.2	88.1	99.4	105.5	16.2	68.7	104.8	119.7	132.1	136.8	9.8	40.8	68.8	83.6	96.8	105.1	12.2	63.1	110.2	137.8	160.8	174.8
HRI	7.4	44.5	73.9	88.2	100.1	106.5	13.7	63.8	101.9	118.4	132.7	138.8	8.6	39.0	67.4	82.9	96.5	105.0	10.2	58.5	107.6	136.8	161.4	178.2
PGBIG	7.2	43.3	73.1	88.8	100.5	106.1	13.4	63.1	100.4	117.7	130.5	136.1	8.4	38.3	66.3	82.0	95.4	103.3	9.8	56.5	101.5	127.8	149.9	165.3
Ours	7.0	46.9	70.6	79.8	90.7	100.3	13.0	68.8	98.2	106.2	116.4	126.1	8.0	39.6	65.1	77.3	88.8	98.0	9.0	59.7	99.5	120.3	138.5	154.1
scenarios	Purchases						Sitting						Sitting Down						Taking Photo					
millisecond	80	320	560	720	880	1000	80	320	560	720	880	1000	80	320	560	720	880	1000	80	320	560	720	880	1000
Res. Sup.	28.7	86.9	122.1	137.2	148.0	154.0	23.8	78.0	113.7	130.5	144.4	152.6	31.7	96.7	138.8	159.0	176.1	187.4	21.9	74.0	110.6	128.9	143.7	153.9
convSeq2Seq	20.3	76.5	111.3	129.1	143.1	151.5	13.5	52.0	82.4	98.8	112.4	120.7	20.7	70.4	106.5	125.1	139.8	150.3	12.7	52.1	84.4	102.4	117.7	128.1
LTD	15.2	64.9	99.2	114.9	127.1	134.9	10.4	46.6	79.2	96.2	110.3	118.7	17.1	63.6	100.2	118.2	133.1	143.8	9.6	43.3	75.3	93.5	108.4	118.8
HRI	13.0	60.4	95.6	110.9	125.0	134.2	9.3	44.3	76.4	93.1	107.0	115.9	14.9	59.1	97.0	116.1	132.1	143.6	8.3	40.7	72.1	90.4	105.5	115.9
PGBIG	12.9	60.1	95.6	111.1	123.1	130.6	9.0	42.5	74.7	91.3	105.2	114.0	14.5	58.0	95.7	114.9	130.1	140.8	8.1	40.1	72.0	90.2	105.2	115.4
Ours	12.1	60.9	88.9	100.0	112.3	123.3	8.7	43.8	71.3	85.2	98.5	108.1	14.1	61.3	94.2	110.3	124.6	135.7	8.2	42.6	70.5	84.8	96.5	106.9
scenarios	Waiting						Walking Dog						Walking Together						Average					
millisecond	80	320	560	720	880	1000	80	320	560	720	880	1000	80	320	560	720	880	1000	80	320	560	720	880	1000
Res. Sup.	23.8	75.8	105.4	117.3	128.1	135.4	36.4	99.1	128.7	141.1	155.3	164.5	20.4	59.4	80.2	87.3	92.8	98.2	25.0	77.0	106.3	119.4	130.0	136.6
convSeq2Seq	14.6	58.1	87.3	100.3	110.7	117.7	27.7	90.7	122.4	133.8	151.1	162.4	15.3	53.1	72.0	77.7	82.9	87.4	16.6	61.4	90.7	104.7	116.7	124.2
LTD	10.4	47.9	77.2	90.6	101.1	108.3	22.8	77.2	107.8	120.3	136.3	146.4	10.3	39.4	56.0	60.3	63.1	65.7	12.2	50.7	79.6	93.6	105.2	112.4
HRI	8.7	43.4	74.5	89.0	100.3	108.2	20.1	73.3	108.2	120.6	135.9	146.9	8.9	35.1	52.7	57.8	62.0	64.9	10.4	47.1	77.3	91.8	104.1	112.1
PGBIG	8.4	42.4	71.0	84.6	95.6	103.2	19.9	72.8	105.5	119.4	135.5	146.1	8.8	35.4	54.4	61.0	64.8	67.4	10.3	46.6	76.3	90.9	102.6	110.0
Ours	7.9	46.2	74.1	84.8	93.4	101.4	18.9	74.7	101.9	111.5	126.3	139.6	8.5	36.0	48.5	49.9	53.3	57.9	9.9	48.8	73.7	84.0	94.3	103.3

TABLE X: Comparison with deterministic models on Human3.6M [22] Setting-B in FDE (mm) at different prediction horizons in different actions. The best results are highlighted in bold, and the second-best ones are marked with underscores.